Nonlinear response of single-molecule nanomagnets: Equilibrium and dynamical

R. López-Ruiz, F. Luis, V. González, A. Millán, and J. L. García-Palacios
Instituto de Ciencia de Materiales de Aragón y Dep. de Física de la Materia Condensada, C.S.I.C., Universidad de Zaragoza, E-50009 Zaragoza, Spain

(Received 11 August 2005; published 27 December 2005)

We present an experimental study of the *nonlinear* susceptibility of Mn_{12} single-molecule magnets. We investigate both their thermal-equilibrium and dynamical nonlinear responses. The equilibrium results show the sensitivity of the nonlinear susceptibility to the magnetic anisotropy, which is nearly absent in the linear response for axes distributed at random. The nonlinear dynamic response of Mn_{12} was recently found to be very large, displaying peaks reversed with respect to classical superparamagnets [F. Luis *et al.*, Phys. Rev. Lett. **92**, 107201 (2004)]. Here we corroborate the proposed explanation—the strong field dependence of the relaxation rate due to the detuning of tunnel energy levels. This is done by studying the orientational dependence of the nonlinear susceptibility, which permits us to isolate the quantum detuning contribution. Besides, from the analysis of the longitudinal and transverse contributions we estimate a bound for the decoherence time due to the coupling to the phonon bath, which is much shorter than the energy-level lifetimes.

DOI: 10.1103/PhysRevB.72.224433 PACS number(s): 75.50.Tt, 75.45.+j, 75.40.Gb

I. INTRODUCTION

Superparamagnets are nanoscale solids or clusters with a large net spin ($S \sim 10^1 - 10^4$). This spin is coupled to the environmental degrees of freedom of the host material—e.g., phonons, nuclear spins, or conducting electrons. Due to the dynamical disturbances of the surroundings, the spin may, among other things, undergo a Brownian-type "reversal," overcoming the potential barriers created by the magnetic anisotropy.

Depending on the relation between the reversal time τ and the observation time t_{obs}, different phenomenologies can be found. For $\tau \ll t_{obs}$, the spin exhibits the thermal-equilibrium distribution of orientations as in a paramagnet; the large values of S are the reason for the name *superparamagnetism*. When $\tau \gg t_{obs}$, in contrast, the reversal mechanisms appear *blocked* and the spin stays close to an energy minimum (stable magnetization conditions appropriate for magnetic storage). Finally, under intermediate conditions ($\tau \sim t_{obs}$) one finds *nonequilibrium phenomena* (i.e., magnetic "relaxation").

For large S—for instance, in magnetic nanoparticles[1]—a classical description is adequate.[2] The essential physical ingredients are the thermoactivation over the magnetic anisotropy barriers and the (damped) spin precession.[3] As the spin value is reduced, quantum effects can start to play a role. For moderate spins ($S \sim 10$), as in single-molecule magnets,[4] the quantum nature of the system comes significantly to the fore. For instance, the spin reversal may also occur by tunneling whenever the magnetic field brings into resonance quantum states located at the sides of the barrier (Fig. 1).

Several fundamental problems can be studied on these systems:[5–7] first, the quantum-to-classical transition, with the emergence of classical properties. Single-molecule magnets constitute a model system to study quantum mechanics at a mesoscopic level, while magnetic nanoparticles provide a natural classical limit. Second, one can address the effects of environmental degrees of freedom on a given system. Classically, one faces the rich phenomenology of rotational Brownian motion of the nanoparticle magnetization. In the quantum case the bath coupling not only produces fluctuations and dissipation (allowing the system to relax to thermal equilibrium), but it is also responsible for the decoherence of its quantum dynamics. Thus, single-molecule magnets constitute an important experimental benchmark to test the predictions of the theory of *quantum dissipative systems*[7] (much as Josephson junctions in superconductivity).

The best studied magnetic molecular clusters are those named Mn_{12} and Fe_8, both with $S=10$ in the ground multiplet (for other examples see Ref. 8). To understand their behavior a plethora of theoretical calculations and every conceivable

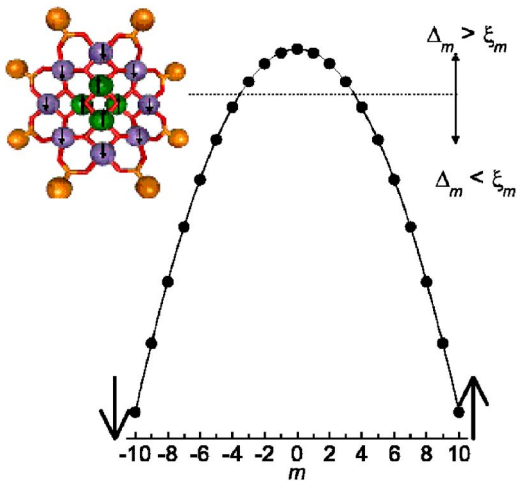

FIG. 1. (Color online) Energy levels for Mn_{12} (the molecule is sketched in the inset along with the spin orientations of the Mn ions). The levels are plotted vs the quantum number m at $H=0$ and show the bistable potential for the spin due to the magnetic anisotropy. The horizontal line marks the border between "classical" or localized energy levels $\Delta_m < \xi_m$ and the tunneling levels $\Delta_m > \xi_m$ (Δ is the tunnel splitting and ξ the width of the environmental bias-field distribution).

experimental technique have been used. However, the nonlinear susceptibility χ_3, fruitfully exploited in studies of spin glasses,[9–11] and random anisotropy systems,[12] but also in magnetic nanoparticles,[13–15] had been overlooked. For *classical* superparamagnets χ_3 provides information on parameters to which the linear susceptibility is less sensitive, like the anisotropy constant D (Ref. 16) or the spin-bath coupling parameter λ (Ref. 17) (which enters the scene due to the strong dependence of the relaxation rate $\Gamma = 1/\tau$ on *transverse* magnetic fields[18]). Besides, the dynamical nonlinear susceptibility has a genuinely *quantum* contribution due to the detuning of the energy levels by a *longitudinal* field.[19] It has a sign opposite to the classical (precessional) contribution, thus allowing us to ascertain whether quantum effects, such as resonant tunneling, are relevant in a given nanomagnet (an issue sometimes controversial[20]).

In this article we present experimental results for the thermal-equilibrium and dynamical nonlinear susceptibility of Mn_{12} acetate. Compared to the linear susceptibility, the equilibrium χ_3 shows an enhanced sensitivity to the magnetic anisotropy, even for axes distributed at random (allowing to estimate D from measurements in powdered samples). As for the frequency-dependent χ_3, we study its dependence on the angle of the applied field. This gives direct access to the relaxation-rate field-expansion coefficients $\Gamma - \Gamma|_{H=0} \propto g_{\|} H_{\|}^2 + g_{\perp} H_{\perp}^2$, which contain valuable information on the spin reversal mechanisms, thus allowing us to separate the "classical-transverse" and "quantum-longitudinal" contributions to χ_3.

In the discussion simple approximate formulas and numerical results from the solution of a Pauli quantum-master equation are used. Our investigation confirms the interpretation of Ref. 19 of the large quantum contribution to $\chi_3(\omega)$ as arising from the detuning of the tunnel channels by a longitudinal magnetic field. Thus, the experimental nonlinear response is consistent with the established scenario[21–26] of thermally activated tunnel via excited states in Mn_{12}. The analysis also gives a bound for the decoherence time τ_Φ (time scale for the attainment of a diagonal density matrix due to the coupling to the phonon bath). The obtained τ_Φ turns out to be much shorter than the lifetime of the spin levels τ_0 and is responsible for a fast loss of coherent dynamics (like tunnel oscillations or precession).

II. SAMPLES AND MEASUREMENTS

A. Samples and setup

Single crystals of Mn_{12} acetate were grown following a procedure similar to that described by Lis.[27] The concentrations of the reactants, however, were higher than those of Ref. 27 in order to increase the supersaturation and growth rate, yielding larger crystals. These were regrown several times by renewing the mother solution. X-ray diffraction patterns of powdered crystals agreed with simulated patterns from the known crystal structure.

The measurements were performed on a single crystal with dimensions $3 \times 0.5 \times 0.5$ mm^3 at different orientations with respect to the applied magnetic field. To this end, we constructed a rotating sample holder that enables the c crystallographic axis (which defines the anisotropy axes of the Mn_{12} molecules) to be rotated a given angle ψ with respect to the magnet axis. This angle is measured with a precision better than 0.5°. To calibrate the position of the zero we used the measured linear equilibrium susceptibility, which should be maximum when the field is parallel to the anisotropy axis ($\psi = 0$).

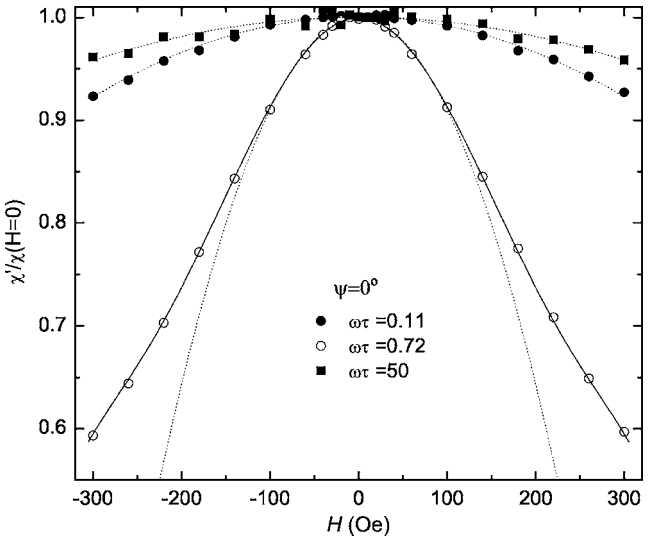

FIG. 2. Magnetic ac susceptibility of a single crystal of Mn_{12}, normalized by its zero-field value, vs the static field H (parallel to the anisotropy axes, $\psi = 0$). Results for the *real part* at $T = 5$ K and various frequencies $\omega\tau$ are shown. The solid lines represent polynomial fits from which χ_3 is obtained. The parabolic approximation $\chi_1 + 3\chi_3 H^2$, which dominates the low-field behavior ($|H| \lesssim 100$ Oe), is shown by dotted lines.

B. Magnetic measurements

Dynamical susceptibility measurements were performed using the ac option of a commercial superconducting quantum interference device (SQUID) magnetometer, by applying an alternating field $\sim \Delta h e^{i\omega t}$. The ac susceptibility was measured under a weak superimposed dc field H, parallel to the oscillating one. The first harmonic of the response can then be expanded as

$$\chi(\omega, H) = \chi_1(\omega) + 3\chi_3(\omega)H^2 + 5\chi_5(\omega)H^4 + \cdots . \quad (1)$$

The (H-independent) expansion coefficients give the ordinary linear susceptibility χ_1 and the nonlinear ones $\chi_3, \chi_5, \ldots$. As it is customary, we focus on χ_3 and refer to it as *the* nonlinear susceptibility.

To determine the nonlinear susceptibility we performed polynomial fits of the H-dependent ac data whose quadratic coefficient gives χ_3. An illustrative example of the fitting procedure is shown in Fig. 2. For sufficiently low H, a good description is provided by a simple parabolic dependence $\chi_1 + 3\chi_3 H^2$. For increasingly larger fields, we increased the order of the polynomials whenever the fitting error became greater than 5%. The experimental χ_3 was taken as the mean value of all quadratic coefficients obtained from the different order polynomials, thus miminizing the error of the determination.

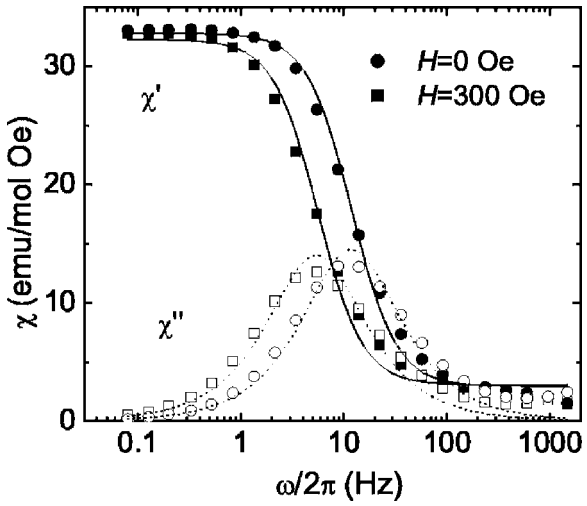

FIG. 3. Magnetic susceptibility vs frequency measured along the anisotropy axis ($\psi=0$) at $T=5$ K. Results are shown at zero bias field (circles) and at $H=300$ Oe (squares). Solid symbols are for the real part (in-phase component) and open symbols for the imaginary part (out-of-phase component). The lines are fits to the Debye law (2) with $\tau|_{H=0}=1.3(3)\times10^{-2}$ s and $\tau|_{H=300}=2.8(1)\times10^{-2}$ s.

The measurements were performed at temperatures in the range $2\ \mathrm{K}<T<45\mathrm{K}$ and frequencies $0.08\ \mathrm{Hz}<\omega/2\pi<1.5$ kHz. The amplitude of the ac field ($\Delta h=3$ Oe) was sufficiently small not to induce nonlinearity in Δh (associated with the generation of harmonics). Actually, the $\chi_3(\omega)$ obtained here from the field-dependent susceptibility differs from the χ_3 extracted from the third harmonic of the response to an ac field (at $H=0$). However, as we show in the Appendix, the dependence of both quantities on the parameters under study is analogous.

C. Equilibrium vs dynamical measurements

In the next sections we are going to study the equilibrium and dynamical susceptibilities. Let us define here a practical criterion to decide when the experimentally measured $\chi_1(\omega)$ and $\chi_3(\omega)$ correspond to equilibrium or off-equilibrium conditions. In the temperature range covered by our experiments, $T>2$ K, the molecular spins of Mn_{12} relax via a thermally activated tunneling mechanism.[21–23] This process gives rise to a well-defined relaxation time τ, and the ac response can be described by a simple Debye formula

$$\chi=\chi_S+\frac{\chi_T-\chi_S}{1+i\omega\tau}. \tag{2}$$

Here χ_T and χ_S are the isothermal (thermal equilibrium) and adiabatic limits of χ. In Fig. 3 we show how the response of the Mn_{12} crystals follows Eq. (2) at temperatures and magnetic fields typical of our experiments.[28] The equilibrium regime corresponds to frequencies fulfilling $\omega\tau\ll1$ (left part of the plot), relaxation effects becoming important when the range $\omega\tau\sim1$ is approached.

On the other hand, the relaxation time of this system increases exponentially as T decreases, following an Arrhenius law (see, for instance, Fig. 2 of Ref. 19)

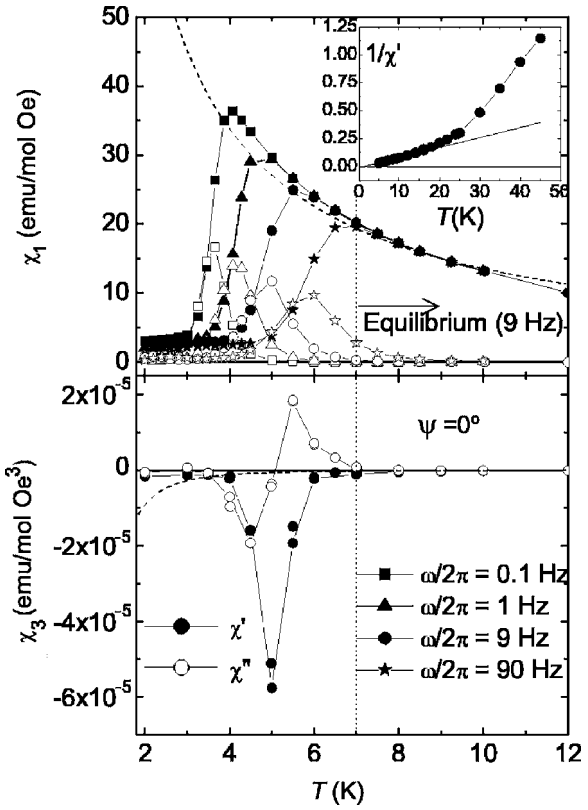

FIG. 4. Linear (top panel) and nonlinear susceptibilities (bottom) vs temperature for several frequencies (only 9 Hz for χ_3) measured along the anisotropy axis. Solid symbols are for the real parts and open symbols for the imaginary parts. Dashed lines are the equilibrium susceptibilities in the Ising (large anisotropy) limit [Eqs. (9) and (10)]. The vertical line marks the boundary above which thermal equilibrium results are safely obtained using $\omega/2\pi=9$ Hz. Inset: temperature dependence of the reciprocal *equilibrium* linear susceptibility and its fit to a Curie-Weiss law (4) for $T<10$ K.

$$\tau=\tau_0\exp(U/k_BT). \tag{3}$$

Here U is an activation energy and τ_0 an attempt time, which set the magnitude and temperature dependence of τ. At zero field we obtained $U_0\simeq65$ K and $\tau_0\simeq3\times10^{-8}$ s.[19] In a χ-vs-T experiment (Fig. 4) the condition $\omega\tau=1$ defines a superparamagnetic "blocking" temperature $k_BT_b=-U_0\ln(\omega\tau_0)$. Below T_b, the real part χ_1' drops from χ_T towards χ_S whereas χ_1'' departs from zero and shows a maximum. As for the nonlinear susceptibility, the nonequilibrium response near T_b leads also to a nonzero imaginary part χ_3'' and to a strong deviation of χ_3' from the equilibrium χ_{3T}. In contrast with the linear response (which decreases from χ_T), χ_3' becomes *larger* than χ_{3T} near T_b (Ref. 19); this dynamical nonlinear phenomenon will be discussed in detail in the following sections.

As can be seen in Figs. 3 and 4, the transition from isothermal to adiabatic conditions extends over a certain frequency or temperature range, determined by the width of the $\chi''(\omega,T)$ curve. As a practical rule, we take $\chi_T=\chi_1'$ and $\chi_{3T}=\chi_3'$ when the imaginary parts are reasonably small

$\chi''/\chi' < 10^{-2}$. This value is, as a matter of fact, close to the experimental error of the present measurements. Using this criterion we have extracted, from the dynamical susceptibility data versus T, the equilibrium χ_T and χ_{3T} discussed in the next section.

III. EQUILIBRIUM LINEAR AND NONLINEAR SUSCEPTIBILITIES

The equilibrium χ_T obtained as described in the previous section is shown in the inset of Fig. 4. In the temperature range $4\ \mathrm{K} < T < 10\ \mathrm{K}$ it approximately follows a Curie-Weiss law

$$\chi_T = \frac{C}{T-\theta}, \tag{4}$$

with a Curie temperature $\theta \simeq 1.2(2)$ K. Measurements performed on a powdered sample (not shown), which are less affected by anisotropy effects, also follow Eq. (4) albeit with a smaller $\theta = 0.5(1)$ K [for the interplay of interactions and anisotropy, see Eqs. (3.2)–(3.6) in Ref. 29]. These finite θ point actually to the presence of dipolar interactions between the molecular spins in the crystal, which would give rise to long-range order at sufficiently low temperatures. In the (super)paramagnetic regime of interest here, interactions merely produce a susceptibility somewhat larger than that of noninteracting clusters.

In addition to interactions, a most important influence on the temperature-dependent susceptibilities is exerted by the magnetic anisotropy.[30] To illustrate these effects, it is helpful to normalize the experimental χ_T and χ_{3T} by their isotropic limits, χ_{iso} and $\chi_{3\mathrm{iso}}$. These can be obtained from the field expansion coefficients of the Brillouin magnetization (Appendix A 1) and read

$$\chi_{\mathrm{iso}} = N_{\mathrm{A}} \frac{(g\mu_{\mathrm{B}})^2 S(S+1)}{3k_{\mathrm{B}}T}, \tag{5}$$

$$\chi_{3\mathrm{iso}} = -N_{\mathrm{A}} \frac{(g\mu_{\mathrm{B}})^4}{45(k_{\mathrm{B}}T)^3} S(S+1)\left[S(S+1)+\frac{1}{2}\right], \tag{6}$$

where N_{A} is the number of molecules per mol. The first of these is merely Curie's law and the second its nonlinear counterpart. Normalized by χ_{iso} and $\chi_{3\mathrm{iso}}$, the experimental susceptibilities lose their bare $1/T$ and $1/T^3$ contributions, so that their remaining temperature dependence is mostly due to the effects of the anisotropy.

The so normalized equilibrium susceptibility data are shown in Fig. 5. Clearly, the isotropic limit is only attained for sufficiently high temperatures ($T \gtrsim 30$ K). Note that the high-T limits of χ_T and χ_{3T} are slightly smaller than χ_{iso} and $\chi_{3\mathrm{iso}}$. This is caused by the thermal population of higher-energy spin multiplets of the cluster, the lowest of which has $S=9$ in Mn_{12}. Therefore, in that temperature range the Mn_{12} molecule can no longer be seen as a superparamagnetic spin $S=10$ and the thermal mixture of spin states reduces its susceptibilities (the analog to the decrease of the spontaneous magnetization in a solid by excitation of spin waves).

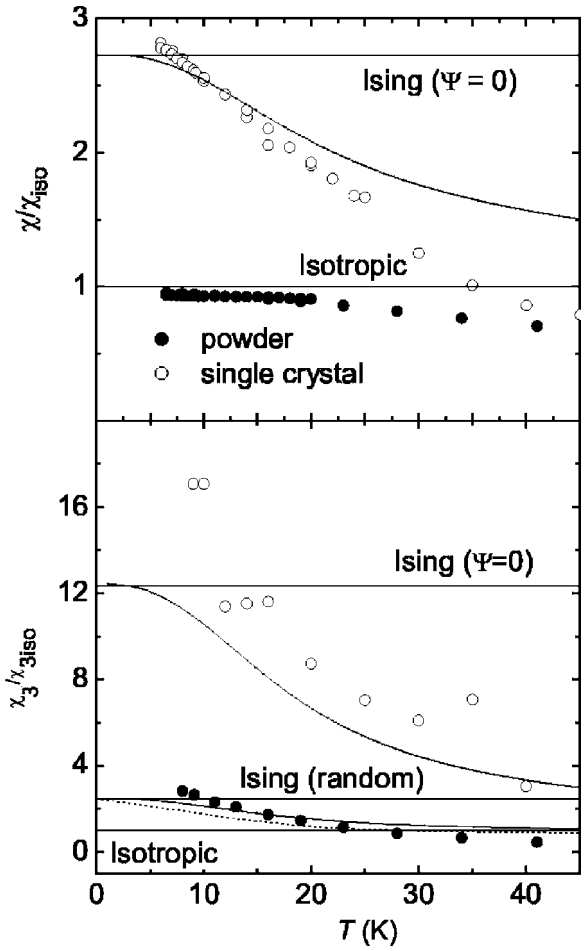

FIG. 5. Temperature dependence of the equilibrium linear and nonlinear susceptibilities normalized by their values for isotropic spins (Brillouin limit). Upper panel: linear susceptibility. Lower panel: nonlinear susceptibility. Results are shown for a single crystal of Mn_{12} with the field parallel to the anisotropy axis (○) and a powder sample (●). The lines are theoretical results for classical spins (dotted line) and quantum spins (solid lines).

As the temperature decreases, both $\chi_T/\chi_{\mathrm{iso}}$ and $\chi_{3T}/\chi_{3\mathrm{iso}}$ increase, departing from $\simeq 1$. This is natural since Eqs. (5) and (6) are only valid when the thermal energy $k_{\mathrm{B}}T$ is larger than all zero-field splittings (produced by the magnetic anisotropy). The simplest Hamiltonian that describes the magnetic behavior of an isolated Mn_{12} molecule contains the Zeeman plus uniaxial anisotropy terms (see also Fig. 1)

$$\mathcal{H} = -DS_z^2 - A_4 S_z^4 - g\mu_{\mathrm{B}}(H_x S_x + H_y S_y + H_z S_z). \tag{7}$$

Here $D \simeq 0.6$ K and $A_4 \simeq 10^{-3}$ K are the second- and fourth-order anisotropy constants for Mn_{12} (Ref. 31) and $H_{x,y,z}$ the components of the field along the (a,b,c) crystallographic axes. The largest zero-field splitting produced by the anisotropy occurs between the states $m = \pm(S-1)$ and the ground state $m = \pm S$:

$$\Omega_0 = (2S-1)D + [S^4 - (S-1)^4]A_4 \simeq 14.8\mathrm{K}. \tag{8}$$

When $k_{\mathrm{B}}T$ becomes comparable to Ω_0 several related effects occur: (i) the magnetization is no longer given by the Bril-

louin law and T does not appear in the combination H/T, (ii) χ_T and χ_{3T} deviate from the simple equations (5) and (6) and depend on ψ, and (iii) the normalized susceptibilities acquire a dependence on T. For classical spins, these effects were studied in Ref. 32.

Eventually, in the low-temperature limit $k_BT/D \to 0$, only the states $m=\pm S$ are appreciably populated and each molecular spin becomes effectively a two-level system ("spin-up" and "spin-down" states). In this "Ising" limit, χ_T and χ_{3T} can also be calculated explicitly:

$$\chi_{\mathrm{Ising}} = N_A \frac{(g\mu_B)^2 S^2}{k_B T} \cos^2 \psi, \tag{9}$$

$$\chi_{3\mathrm{Ising}} = -N_A \frac{(g\mu_B)^4 S^4}{3(k_B T)^3} \cos^4 \psi. \tag{10}$$

Here we see that the bare $1/T$ and $1/T^3$ dependences are recovered, so that the normalized susceptibilities become again temperature independent. Comparison of these expressions with Eqs. (5) and (6) reveals that, for a single crystal at $\psi=0$, $\chi_T/\chi_{\mathrm{iso}}$, and $\chi_{3T}/\chi_{3\mathrm{iso}}$ should increase, respectively, by an overall factor of 2.7 $[=3\times S^2/S(S+1)]$ and 12.3 $(=15\times S^4/S(S+1)\left[S(S+1)+\frac{1}{2}\right])$, when decreasing temperature. The experimental curves approach indeed these values at low temperatures ($T<10$ K in Fig. 5), although they become even larger. This is probably due to the interactions which, as we have seen, enhance the magnetic response at low temperatures.

Anyhow, these results suggest the measurement of the temperature-dependent reduced susceptibilities as a suitable tool to estimate the anisotropy parameters of superparamagnets. In this respect, the advantage of the nonlinear susceptibility becomes evident when dealing with systems with randomly oriented axes. Then the ratios between the "Ising" and isotropic limits decrease significantly [cf. Eqs. (5) and (6) with Eqs. (9) and (10)]. Indeed, $\chi_T/\chi_{\mathrm{iso}}$ becomes nearly T independent, whereas the reduced nonlinear susceptibility still retains a sizable variation with T (by a factor ~ 2.5). This is experimentally confirmed by measurements on a polycrystalline sample (Fig. 5).[33] Thus we see that, contrary to the linear response, χ_{3T} keeps information on the anisotropy even for superparamagnets with axes distributed at random. This is the case most often encountered in nanoparticle systems[1] but also for single-molecule magnets when deposited on surfaces[34] or inside porous materials.[35]

The considerations above can be supported by direct diagonalization of the Hamiltonian (7). The results (solid lines in Fig. 5) exhibit the same trends as the experiments, both for parallel axes and after averaging over random orientations. Full agreement is precluded by the effect of interactions, on the low-T side, and by the population of excited multiplets with $S\neq 10$ at high T, as discussed above.

Before concluding this section, there is an additional feature that deserves to be commented upon. Consider the theoretical behavior of χ_{3T} in *classical* spins, also plotted in Fig. 5.[36] We see that, although classical and quantum calculations predict the crossover from the isotropic to the Ising limits, the classical susceptibilities are shifted towards lower temperatures. This shift can be seen as a manifestation of the quantum, discrete nature of the energy spectrum of Mn_{12}. The finite energy gap between the two lowest quantum levels, Ω_0, leads to a faster (exponential in D/T) convergence to the Ising limit, whereas classically this limit is only approached with a slow power law in D/T (see Appendix A 2).

IV. DYNAMICAL SUSCEPTIBILITIES

In this section we turn our attention from the equilibrium to the dynamical response. We begin reviewing briefly the behavior of the nonlinear susceptibility χ_3 in the *classical* case. This allows us to introduce some basic expressions valid also for quantum superparamagnets; then we present the experimental results for Mn_{12}.

A. Classical superparamagnets and modelization

The dynamical nonlinear susceptibility of classical spins was theoretically found to be very large and, in contrast to the linear susceptibility, nontrivially sensitive to the spin-bath coupling strength λ.[17,37] The "damping" λ measures the relative importance of the relaxation and Hamiltonian (precessional) terms in the dynamical equations.[2,32] Thus $1/\lambda$ is of the order of the number of precessional turns that the spin executes in the deterministic spiraling down to the energy minima.

The contributions to the nonlinear response of the longitudinal and transverse components of the field are captured by a simple formula involving the low-H expansion coefficients $g_\parallel$ and $g_\perp$ of the relaxation rate[38]

$$\Gamma \simeq \Gamma_0 \left[1 + \frac{1}{2}(g_\parallel \xi_\parallel^2 + g_\perp \xi_\perp^2) \right], \tag{11}$$

where $\Gamma_0=\Gamma|_{H=0}$ and $\xi=g\mu_B SH/k_BT$.[39] The expression for the nonlinear susceptibility oscillating with the third harmonic of the field[37] can be found in Appendix A 3. It is easy to find the counterpart for the χ_3 oscillating with $e^{\pm i\omega t}$, as used in this work, which reads

$$\chi_3 = -N_A \frac{(g\mu_B)^4 S^4}{3(k_B T)^3} \left[\frac{\cos^4 \psi}{1+i\omega\tau} - \frac{i\omega\tau}{2(1+i\omega\tau)^2} (g_\parallel \cos^4 \psi + g_\perp \cos^2 \psi \sin^2 \psi) \right]. \tag{12}$$

Here the Ising approximation for the equilibrium parts has been used (this works fine at temperatures around the blocking temperature $T_b \sim 5$ K; see Sec. III). The longitudinal part, proportional to $\cos^4 \psi$, is maximum at $\psi=0$ (in absolute value); the "transverse" contribution associated with $g_\perp$ becomes zero both at $\psi=0$ and $\pi/2$, being maximum at $\psi=\pi/4$. Equation (12) shows that the magnitude, signs, and ω and angular dependences of χ_3 are determined by the competition between the rate expansion coefficients $g_\parallel$ and $g_\perp$. Therefore, measurements of those dependences can provide valuable information on the different contributions to the spin reversal.

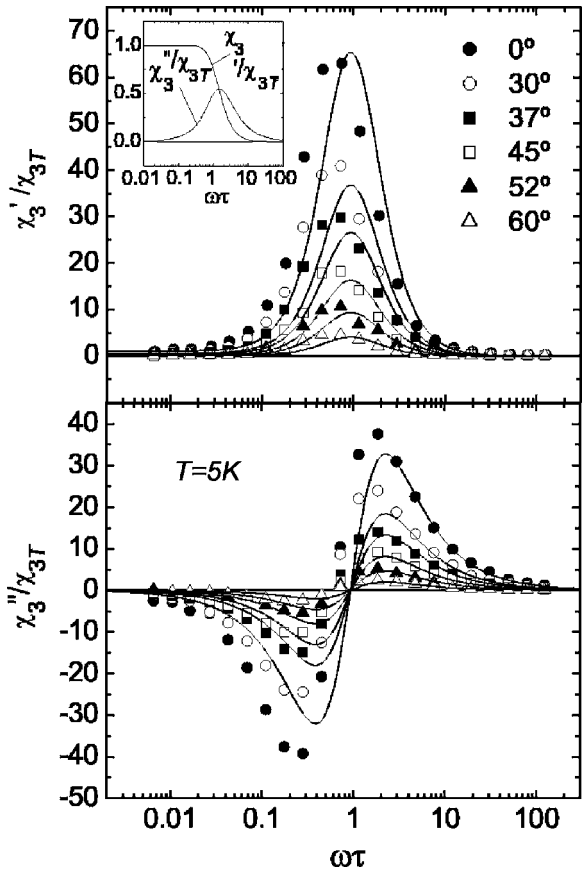

FIG. 6. Nonlinear susceptibility vs frequency at $T=5$ K. Results are shown for different angles ψ between the applied field and the anisotropy axis. The data are normalized by the equilibrium χ_{3T} measured at $\psi=0$. The relaxation time τ was obtained from ω-dependent linear susceptibility measurements (as those of Fig. 3). Upper panel: real part χ_3'. Lower panel: imaginary part χ_3''. The lines are obtained using Eq. (12) with $g_\parallel=-260$ and $g_\perp=0$. The inset shows the sharply different classical prediction for $\psi=0$.

For classical superparamagnets, where only the thermoactivation operates, the rate expansion coefficients are given in the considered low-temperature range by[37,38]

$$g_\parallel = 1, \quad g_\perp = F(\lambda)/2, \tag{13}$$

where $F>0$ is a function of λ (and T). For strong damping, $F\to 1$, so that $g_\parallel$ and $g_\perp$ are of the same order. In contrast, in the weak-damping regime (governed by the precession), one has $F\propto 1/\lambda$ and $g_\perp$ becomes very large, dominating the nonlinear response. Then one can find that the real part $|\chi_3'|\gg|\chi_{3T}|$ but with $\chi_3'/\chi_{3T}<0$ (i.e., the sign is reversed with respect to the equilibrium value). This phenomenology is equivalent to that of the third-harmonic nonlinear susceptibility,[17,37] since both quantities exhibit similar dependences on λ and ω.

It is worth mentioning that in the derivation of Eq. (12) rather general assumptions are invoked (Appendix A 3). Therefore, the functional form obtained is quite generic and valid for classical as well as quantum superparamagnets. Then, the relevant information on the quantum reversal mechanisms will be incorporated by the rate expansion coefficients $g_\parallel$ and $g_\perp$. Naturally, they could be very different from their classical counterparts (13).

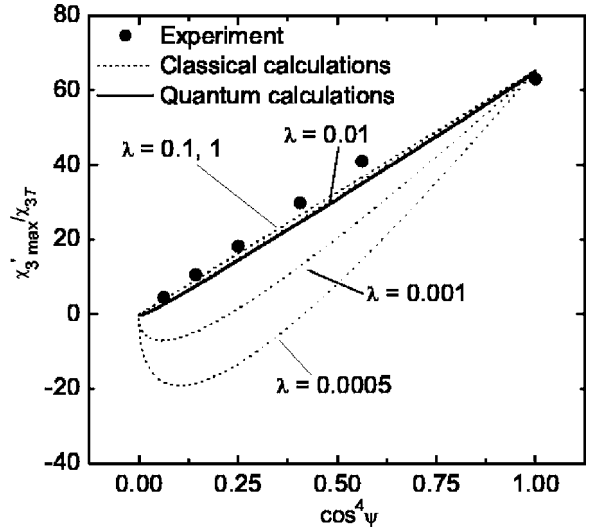

FIG. 7. Evolution of the maximum of $\chi_3'(\omega)$ with the angle ψ of the applied field at $T=5$ K. The symbols are the experimental results. The dashed lines are obtained from Eq. (12) using the experimentally determined $g_\parallel=-260$ and the classical transverse contribution $g_\perp=F(\lambda)/2$ computed for different values of the phenomenological damping constant λ. The solid line corresponds to theoretical calculations with a Pauli quantum master equation (see the text).

B. Nonlinear dynamical susceptibility of Mn_{12}

After these theoretical considerations let us turn to the experiments on quantum nanomagnets. Figure 6 displays frequency-dependent measurements of the nonlinear susceptibility of Mn_{12} performed at constant T for different angles ψ. They demonstrate that the result already shown in Fig. 4—namely, that χ_3' becomes much larger than its equilibrium value χ_{3T} near the blocking temperature—is a dynamical effect not caused by magnetic ordering or some kind of "freezing" (interactions also enhance the susceptibilities, but by a much smaller factor). We know that classically one can also have $|\chi_3'|\gg|\chi_{3T}|$, but here $\chi_3'/\chi_{3T}>0$; that is, the peak of the measured nonlinear dynamic susceptibility is *reversed* with respect to the classical prediction.

From Eq. (12) we see that at $\psi=0$ there is no contribution of $g_\perp$ to χ_3. In addition, the first term in that equation, which has a Debye-type profile, cannot provide $|\chi_3'|>|\chi_{3T}|$ because $\mathrm{Re}[\chi/(1+ix)]\leqslant\chi$. Therefore, the maximum observed in Fig. 6 should be due to the $g_\parallel$ contribution. There is a result relating the height of the susceptibility peak $\chi_3'|_{\max}$ with the combination $Q(\psi)\equiv g_\parallel\cos^2\psi+g_\perp\sin^2\psi$ of the relaxation rate coefficients (Appendix A 3)

$$\chi_3'|_{\max}/\,\chi_{3T}|_{\psi=0} \simeq -\cos^2\psi Q(\psi)/4. \tag{14}$$

Therefore, the positive sign of the maximum of $\chi_3'(\omega)/\chi_{3T}$ at $\psi=0$ entails $Q<0$. But $Q|_{\psi=0}=g_\parallel$, entailing that the relaxation time $\tau=1/\Gamma$ becomes *longer* as $H_\parallel$ increases. No clas-

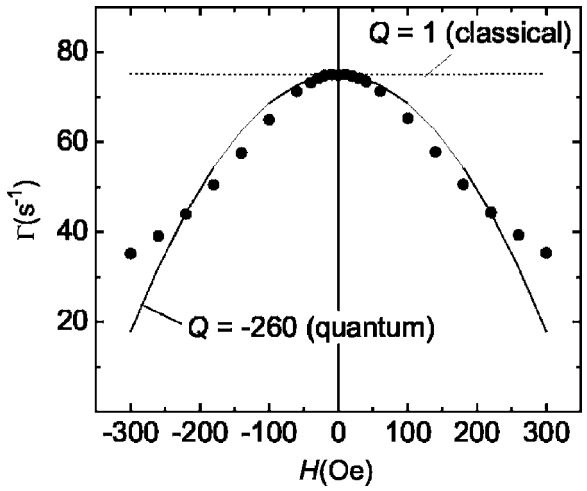

FIG. 8. Relaxation rate of Mn_{12} at $T=5$ K as a function of the field applied along the anisotropy axis ($\psi=0$). The symbols are the Γ's obtained from Debye fits of $\chi(\omega,H)$. The lines are calculated as $\Gamma=\Gamma_0(1+Q\xi^2/2)$, where $\xi=g\mu_B SH_\parallel/k_BT$ and Q comes from the maximum of $\chi_3'(\omega)$ via Eq. (14). The classical prediction ($Q=1$) is shown for comparison.

sical mechanism can account for this; actually, $g_\parallel=1$ in the classical model, which gives a $\chi_3'/\chi_{3T}|_{\psi=0}$ smaller than 1 and decreasing with ω (inset of Fig. 6), in sharp contrast to the measured χ_3. On the other hand, it is well established[21–26] that in Mn_{12} the suppression of tunneling by a longitudinal field *strongly* reduces the relaxation rate (as it breaks the degeneracy between initial "spin-up" and final "spin-down" states, inhibiting the tunnel channels). As suggested in Ref. 19 this effect provides the $g_\parallel$ required, both negative and large, to account for the experimental χ_3 of Mn_{12}. Thus, we see that the known field suppression of tunneling shows up in the nonlinear response as a distinctly quantum contribution, with its sign reversed with respect to the classical case.

When $\psi>0$, the detuning quantum contribution coexists with the transverse $g_\perp$ contribution. Still, the data of Fig. 6 suggest that $\chi_3\propto\cos^4\psi$ holds approximately. We can check this by accounting again for Eq. (14) and plotting the maximum of χ_3' vs $\cos^4\psi$ (Fig. 7). This yields an almost straight line indicating that in Mn_{12} the coefficient $g_\parallel$ overwhelmingly dominates $g_\perp$, which in the classical case embodied the precessional contribution and could be sizable (we return to this issue in Sec. V).

Thus $\chi_3(\omega,\psi)$ provides *direct* experimental access to the relaxation-rate expansion coefficients $g_\parallel$ and $g_\perp$, which contain information on the spin relaxation mechanisms. Besides, from the sign of the $\chi_3(\omega)$ peaks we can infer whether the spin reversal is dominated by a classical mechanism or by quantum processes. The consistency of our analysis can be ascertained by comparing the experimentally determined rate Γ (obtained from Debye fits of χ), with the rate reconstructed from the expansion $\Gamma=\Gamma_0(1+Q\xi^2/2+\cdots)$, using the $Q|_{\psi=0}$ extracted from the χ_3' maxima via Eq. (14) ($Q_{Mn_{12}}|_{\psi=0}\simeq-260$). Figure 8 shows the good agreement between both results in the weak-field regime, supporting our interpretation.

V. DISSIPATION vs DECOHERENCE IN SINGLE-MOLECULE MAGNETS

We have seen in the previous section that the transverse contribution to the nonlinear susceptibility is nearly absent in Mn_{12} (indeed the experiments are consistent with $g_\perp=0$). Classically, $g_\perp$ incorporates the precessional contribution, which can be large for weak damping $\lambda\ll1$.[17,37] Still, as its long τ_0 indicates, Mn_{12} is expected to be quite "underdamped" (in the sense of energy dissipation). Thus, it seems that some other process makes the spin to lose its intrinsic, or coherent, precessional dynamics and appear, when seen through $\chi_3(\omega)$, as "overdamped." In this last section we will try to reconcile these results ($g_\perp\simeq0$ and long τ_0), invoking an effect of the coupling to the bath absent in classical physics: *decoherence*.

A. Experimental bound for the effective damping

Before starting let us quantify a lower bound for an effective λ of Mn_{12}. To this end we generate $\chi_3(\omega)$ curves using Eq. (12) with the $g_\parallel$ experimentally determined from $\chi_3(\omega)|_{\psi=0}$, while assuming $g_\perp=F(\lambda)/2$ as in classical superparamagnets. In this way we compute $\chi_3'|_{max}$ vs $\cos^4\psi$ for several λ and compare with the experimental results (Fig. 7). The best agreement is obtained for large λ, which in fact yields small $g_\perp$ and hence almost no $\cos^2\psi\sin^2\psi$ contribution. However, taking into account experimental uncertainties as well as the smaller sensitivity of $g_\perp$ to large λ gives a lower bound of $\lambda\gtrsim0.01$.

In the classical equations of motion the damping parameter λ is a measure of the relative weights of their relaxation and precessional terms. It can then be expressed as the Larmor precession period $\tau_L=2\pi/\gamma H_a$ (in the anisotropy field H_a; $\gamma=g\mu_B/\hbar$) divided by some time scale of relaxation. For the latter we can use the classical prefactor in the Arrhenius law[2,32]

$$\tau_0=\frac{1}{\lambda\gamma H_a}\sqrt{\frac{\pi}{4\sigma}}\left(1+\frac{1}{\sigma}+\cdots\right), \tag{15}$$

where the reduced anisotropy barrier is $\sigma=U_0/k_BT$. In our experiments at $T=5$ K we have $\sigma\simeq14$, whence

$$\lambda\simeq0.04\times\tau_L/\tau_0. \tag{16}$$

Experimentally $\tau_0\sim3\times10^{-8}$ s in Mn_{12}. Its anisotropy field can be obtained from magnetization measurements (along the hard plane) or from the ground-state transition frequency $\Omega_0/\hbar$ [Eq. (8)], getting $\tau_L\simeq3$–4×10^{-12} s. This gives $\tau_L/\tau_0\sim10^{-4}$ and hence an effective λ many orders of magnitude smaller than the lower bound $\lambda\gtrsim0.01$ extracted from χ_3.

The estimation of τ_L/τ_0 is in agreement with the mentioned underdamped character of Mn_{12} (in the sense of long-lived levels). However, in case of $g_\perp$ having some precession-type contribution akin to $F(\lambda)$, the above $\lambda\propto\tau_L/\tau_0$ would not be the parameter entering there. Otherwise a giant $g_\perp\propto1/\lambda$ would dominate χ_3 (leading to $\chi_3'/\chi_{3T}<0$ and $\chi_3'|_{max}$ not proportional to $\cos^4\psi$), which is clearly not seen in the experiments. Still, it might be that,

instead of the damping, some other time scale limits the precession; as this is a type of coherent dynamics, we can call such time a decoherence time $\tau_{\rm dec}$. This should replace τ_0 in the effective $\lambda \propto \tau_{\rm L}/\tau_{\rm dec}$. To get a λ consistent with the lower bound $\lambda \gtrsim 0.01$ obtained from χ_3, the time $\tau_{\rm dec}$ should be far shorter than $\tau_0 \sim 10^{-8}$ s, actually we get $\tau_{\rm dec} \sim 1-1.5\times 10^{-11}$ s.

B. Approximate quantum treatment

A critical assessment of the considerations above is in order before proceeding. They have been based on stretching the classical idea that $g_\perp$ should include some precessional-type contribution. Further, they assume that this contribution is controlled by a parameter relating the Larmor period with some scale limiting the time allowed to the spin to precess (either by damping or by some loss of coherence). By definition, however, $g_\perp$ accounts for the effects of $H_\perp$ on the relaxation rate [Eq. (11)]; besides, $\chi_3(\omega)$ gives *direct* access to $g_\parallel$ and $g_\perp$. Then, one would expect that a pure quantum approach for Γ, including the bath coupling and coherent dynamics (tunnel and precession), could account for the experimental χ_3 without recourse to classically preconceived notions.

An exact quantum treatment, unfortunately, is difficult because one must deal with the full density-matrix equation including the intrinsic (Hamiltonian) dynamics plus the effects of the bath (damping and decoherence). However, as this can be handled in various limit cases, we shall attempt a discussion based on the corresponding partial solutions for the quantum Γ, with the hope of shedding some light on the physical origin of the results.

The dominant terms that enter the relaxation rate describing quantum tunneling via a pair of nearly degenerate states $|\pm m\rangle$ have a Lorentzian shape as a function of the *longitudinal* bias $\xi_m = 2mg\mu_{\rm B}H_\parallel$ (Ref. 40):

$$\Gamma \simeq 2\Gamma_m \frac{\Delta_m^2}{\xi_m^2 + \underbrace{\Delta_m^2 + \hbar^2\Gamma_m^2}_{w_m^2}} \exp(-U_m/k_{\rm B}T). \tag{17}$$

Here Γ_m is the probability of decaying to other levels via the absorption or emission of phonons (i.e., it is approximately $1/\tau_0$), Δ_m is the tunnel splitting of the pair $|\pm m\rangle$ induced by terms not commuting with S_z in the Hamiltonian, and U_m is the energy of the levels. The width of the Lorentzian introduced,[41] $w_m^2 = \Delta_m^2 + \hbar^2\Gamma_m^2$, interpolates between the results that can be obtained in the two limit cases of (i) large coupling $\hbar/\tau_0 \gg \Delta_m$,[24] where $w_m \simeq \hbar/\tau_0$, and (ii) weak coupling $\hbar/\tau_0 \ll \Delta_m$,[25] in which $w_m \simeq \Delta_m$.

Performing the second $H_\perp$ derivative of Eq. (17) gives the corresponding $g_\perp$. For the parameters of Mn_{12} it results that the main contribution at zero longitudinal bias comes from the derivative of the quotient Δ_m^2/w_m^2:

$$g_\perp \equiv \left.\frac{1}{\Gamma_0}\frac{\partial^2\Gamma}{\partial H_\perp^2}\right|_0 \simeq \frac{2}{(\Delta_m/w_m)}\frac{\partial^2}{\partial H_\perp^2}(\Delta_m/w_m). \tag{18}$$

Now, for large coupling $\hbar/\tau_0 \gg \Delta_m$, we have $w_m = \hbar/\tau_0$. Then the relaxation rate depends on the ratio between τ_0 and the tunneling time $\hbar/\Delta_m$. A transverse field eases the tunneling and significantly increases Δ_m, and hence Γ. As Γ is then quite sensitive to $H_\perp$, we can have large $g_\perp$, in analogy with the classical situation. On the contrary, when $\hbar/\tau_0 \ll \Delta_m$, we have $w_m \simeq \Delta_m$ and hence $\Delta_m^2/w_m^2 \simeq 1$. Then the rate becomes quite insensitive to Δ_m (and hence to $H_\perp$), leading to a small $g_\perp$.

In Mn_{12}, where $\hbar/\tau_0 \sim 0.2$ mK, both situations are possible. The reason is the exponential increase of the tunnel splitting Δ_m with decreasing $|m|$, going from the sub-nanokelvin regime for the ground levels $m = \pm S$ to some tenths of K for $|m| \lesssim 2$. Therefore, the relation between $\hbar/\tau_0$ and Δ_m depends on which tunneling path (i.e., which pair $\pm m$) gives the dominant contribution to Γ. If tunneling proceeds via the deep levels, where $\hbar/\tau_0 \gg \Delta_m$, we would find a large $g_\perp$. In contrast, when tunneling occurs through the excited levels, one has $\hbar/\tau_0 \ll \Delta_m$ and hence small $g_\perp$.

At this point it is important to bring into the discussion the effect of environmental bias fields (due to intermolecular dipolar interactions or the hyperfine interaction with the nuclear spins of the Mn ions). They produce a distribution of bias ξ whose typical width is of a few tenths of K (of the order of the Curie-Weiss θ). These bias fields enter as $\Delta_m^2/(\xi_m^2 + w_m^2)$ in the rate expression (17), replacing the bare Δ_m^2/w_m^2 and supressing tunneling when $w_m \ll \xi_m$ (Fig. 1). Taking into account the order of magnitude of ξ_m, the bias effectively blocks tunneling via the large $|m|$ (deep) channels, those that would provide large $g_\perp$. Tunneling becomes possible only for $\Delta_m > \xi_m$, but for those upper levels $\hbar/\tau_0 \ll \Delta_m$, leading to small $g_\perp$, in agreement with the experiments.

We can support this picture with direct numerical calculations. An approximate (Pauli) quantum master equation, which works well when tunneling occurs under weak-damping conditions and that incorporates the effects of environmental bias fields, was used to study several problems in Mn_{12}.[25,42,43] We have implemented it to address the nonlinear response problem, mimicking the experimental protocol and calculating χ' and χ'' vs H. Results are shown in Fig. 7 (solid line; see also Fig. 3 of Ref. 19). They account well for the measured nonlinear susceptibility, in particular for the nearly $\cos^4\psi$ dependence of χ_3 associated with small $g_\perp$.

We would like to also provide a physical picture in the limit cases discussed ($\hbar/\tau_0$ much larger or smaller than Δ_m). To this end, let us discuss the total energy of the spin plus the bath, treating their interaction perturbatively. Then, time-dependent perturbation theory leads to the celebrated *time-energy* "uncertainty" relation. In particular, for $t \gtrsim \hbar/\Delta E$ the dominant transitions are those conserving the total energy. On the other hand, for a spin in a $|m\rangle$ state, which is not an exact eigenstate of the Hamiltonian, the energy uncertainty is of the order of the tunnel splitting Δ_m. Well, consider now a transition to such an $|m\rangle$ state; although the spin could at short times remain there, for times longer than $\tau_\Phi \equiv \hbar/\Delta_m$ it will have to become an energy eigenstate. Then the wave function consists of a superposition of spin-up and spin-down states $|\pm m\rangle$, delocalized between both sides of the barrier.

We can now reexamine the limit cases discussed above. Consider first the strong-coupling case $\hbar/\tau_0 \gg \Delta_m$. For times shorter than the decay τ_0, the time-energy uncertainty allows

the existence of superpositions of energy eigenstates, which can be localized on either side of the barrier ($\sim|\pm m\rangle$). These wave packets may exhibit Hamiltonian dynamics including tunnel oscillations and precession. Under these conditions the rate Γ is quite sensitive to Δ_m, as it controls the probability for the spin to have tunneled before a time τ_0. It is this sensitivity to Δ_m, and in turn to $H_\perp$, which can lead to large $g_\perp$.

When, by constrast, $\hbar/\tau_0 \ll \Delta_m$ the "semiclassical" wave packet around $|m\rangle$ delocalizes in the tunneling time, $\tau_\Phi = \hbar/\Delta_m$, evolving towards an energy eigenstate due to the uncertainty principle. Then, there is no coherent oscillation between $|m\rangle$ and $|-m\rangle$, neither precession of the (averaged) transverse components, since this is a stationary state. The dependence on Δ_m (and hence on $H_\perp$) is then minimized, as the wave function is already delocalized between the spin-up and spin-down states, leading to small $g_\perp$ values. Note that under these conditions the coherent (precessional) dynamics is not limited by the level lifetime τ_0 but by the much shorter "decoherence" time to attain a diagonal density matrix. Therefore, the $\tau_{\rm dec}$ introduced heuristically above can be identified with this $\tau_\Phi = \hbar/\Delta_m$. For $|m| = 2,4$, we have $\Delta_m \sim 0.7$–0.02 K, which give $\tau_\Phi \sim 10^{-11} - 4\times 10^{-10}$ s. These values are consistent with the estimation, based on $\chi_3(\omega)$, of the $\tau_{\rm dec}$ required to get $\lambda \sim 0.01$ (which yielded $\tau_{\rm dec} \sim 10^{-11}$ s).[44]

VI. SUMMARY AND CONCLUSIONS

The single-molecule magnet Mn_{12} is a model system for the study of thermal-equilibrium properties of spins with magnetic anisotropy, as well as the dynamics of a quantum mesoscopic system subjected to the effects of a dissipative environment. In this system, to the rich physics of classical supeparamagnets, quantum effects are incorporated. In this article we have investigated experimentally the equilibrium and dynamical nonlinear responses of Mn_{12}. The nonlinear susceptibility χ_3 was underexploited in this field in spite of having, when compared to the linear susceptibility, an enhanced sensitivity to several important characteristics of the system.

We have shown the sensitivity of the *equilibrium* χ_3 to the magnetic anisotropy parameters of the spin Hamiltonian. As in the classical case, the anisotropy leads to an extra temperature dependence of χ_3, which, in contrast to the linear susceptibility, persists for randomly distributed anisotropy axes. Therefore, the measurement of $\chi_3(T)$ can be exploited to estimate the anisotropy constants even in powdered samples or in systems deposited on surfaces or in porous materials.

The analysis of the *dynamical* χ_3, with help from a generic but simple formula [Eq. (12)], provides valuable information on the intrinsic dynamics of the system. Specifically, $\chi_3(\omega,\psi)$ gives access to the relaxation-rate field-expansion coefficients $g_\parallel$ and $g_\perp$ [Eq. (11)], which contain information on the mechanisms of spin reversal. The experimental nonlinear response of Mn_{12} is found to be consistent with the established scenario of thermally activated tunnel via excited states. Thus, the strong decrease of the relaxation rate due to the (longitudinal) field detuning of tunnel levels manifests itself in χ_3 as a distinct quantum contribution, with a sign opposite to the classical case. Then, from the signs of the χ_3 vs ω peaks one can estimate if quantum effects play a role in the dynamics of the studied nanomagnet. Finally, from the analysis of the angular dependence of $\chi_3(\omega)$ we have estimated a bound for the decoherence time required to attain a diagonal density matrix due to the phonon-bath coupling. The so-obtained τ_Φ is much shorter than the level lifetime τ_0 and is the responsible for a fast loss of coherent dynamics like tunnel oscillations or precession.

ACKNOWLEDGMENTS

This work has been funded by Project Nos. MAT02-0166 and BFM2002-00113 from Ministerio de Ciencia y Tecnología and PRONANOMAG from Diputación General de Aragón (Spain). R.L.R. acknowledges a grant from Consejo Superior de Investigaciones Científicas.

APPENDIX: ANALYTICAL EXPRESSIONS FOR VARIOUS QUANTITIES

In this appendix we derive a number of analytical formulas used in the discussions of the main text: first, the equilibrium nonlinear susceptibility of a spin S in the isotropic limit (from the Brillouin magnetization) and, then, corrections due to finite magnetic anisotropy to the equilibrium linear and nonlinear susceptibilities in the opposite Ising limit. Finally, we derive the frequency-dependent nonlinear susceptibility (12); we also analyze the zeros, extrema, and signs of the formula for $\chi_3(\omega)$. For simplicity, we omit throughout the appendix unessential constants like N_A, $g\mu_B$, k_B, etc.

1. Equilibrium isotropic susceptibilities from the Brillouin magnetization

For isotropic spins, we can get the equilibrium linear and nonlinear susceptibilities by expanding the Brillouin function around a zero field. The isotropic magnetization can be written as ($y = H/T$)

$$M_z = a\coth(ay) - b\coth(by), \quad a = S + \frac{1}{2}, \quad b = \frac{1}{2}.$$

Then, from the first terms of the small-x expansion of the hyperbolic cotangent—namely, $\coth(x) \simeq 1/x + x/3 - x^3/45$—we get

$$M_z \simeq \frac{1}{3}(a^2 - b^2)y - \frac{1}{45}(a^4 - b^4)y^3 \equiv^{\rm def} \chi_T H + \chi_{3T} H^3.$$

Using now $a^2 - b^2 = S(S+1)$ and $a^2 + b^2 = S(S+1) + \frac{1}{2}$, we finally obtain

$$\chi_T = \frac{S(S+1)}{3T}, \quad \chi_{3T} = -\frac{S(S+1)\left[S(S+1)+\frac{1}{2}\right]}{45T^3}. \quad \text{(A1)}$$

The first is the celebrated *Curie law* and the latter its sought

generalization for the nonlinear response. Note that there is no second order χ_2 since M_z is odd in H.

2. Finite-anisotropy corrections to the equilibrium Ising susceptibilities

Now we go into the corrections due to finite anisotropy to the susceptibilities in the opposite Ising limit. In this regime, for uniaxial anisotropy, only the states $m=\pm S$ are populated at zero field, and each cluster becomes effectively a two-level system. We will consider the effects of finite population of the first excited levels $m=\pm(S-1)$. For simplicity and to compare with known results in the classical case,[32] we assume the simplest form for the magnetic anisotropy $\mathcal{H}=-DS_z^2$ [cf. Eq. (7)].

We start from the statistical-mechanical expressions for the susceptibilities at zero field:[16]

$$\chi_T=\frac{\langle S_z^2\rangle}{T},\quad \chi_{3T}=\frac{\langle S_z^4\rangle-3\langle S_z^2\rangle^2}{6T^3}. \tag{A2}$$

To get the equilibrium averages $\langle S_z^k\rangle$, we need first the partition function. Including the contributions of the ground states, $m=\pm S$, and first excited states, $m=\pm(S-1)$, we simply have

$$\mathcal{Z}=\sum_{m=-S}^{S}\mathrm{e}^{-\varepsilon_m/T}\simeq 2(\mathrm{e}^{-\varepsilon_S/T}+\mathrm{e}^{-\varepsilon_{S-1}/T}), \tag{A3}$$

where we have taken into account the zero-field degeneracy $\varepsilon_{-m}=\varepsilon_m$ (yielding the factor of 2). For $\varepsilon_m=-Dm^2$ the separation between adjacent levels is $\varepsilon_m-\varepsilon_{m-1}=-D(2m-1)$. Thus, for the ground-state splitting one has $\varepsilon_S-\varepsilon_{S-1}=-D(2S-1)=-\Omega_0$, which corresponds to Eq. (8). Then, extracting a factor $\mathrm{e}^{-\varepsilon_S/T}$ in $\mathcal{Z}$, we find the approximate partition function for our problem,

$$\mathcal{Z}\simeq 2\mathrm{e}^{-\sigma}(1+\mathrm{e}^{-\Omega_0/T}), \tag{A4}$$

where we have also introduced the reduced anisotropy barrier $\sigma=DS^2/T$.

Next, we compute the moments $\langle S_z^k\rangle\propto\Sigma_m m^k\mathrm{e}^{-\varepsilon_m/T}$ required in Eqs. (A2) within the same approximation:

$$\langle S_z^k\rangle=\frac{2}{\mathcal{Z}}S^k\mathrm{e}^{-\sigma}\left[1+\left(\frac{S-1}{S}\right)^k\mathrm{e}^{-\Omega_0/T}\right]. \tag{A5}$$

We have considered even k, yielding the factor of 2; otherwise, the moments vanish (as they are computed at $H=0$). Then, dividing by $\mathcal{Z}$ as given by Eq. (A4), we have

$$\langle S_z^k\rangle=S^k\frac{1+\left(\frac{S-1}{S}\right)^k\mathrm{e}^{-\Omega_0/T}}{1+\mathrm{e}^{-\Omega_0/T}}. \tag{A6}$$

Inserting these moments for $k=2,4$ into Eqs. (A2), we get

$$\chi_T=\frac{S^2}{T}\frac{1+\left(\frac{S-1}{S}\right)^2\mathrm{e}^{-\Omega_0/T}}{1+\mathrm{e}^{-\Omega_0/T}},$$

$$\chi_{3T}=\frac{S^4}{6T^3}\left\{\frac{1+\left(\frac{S-1}{S}\right)^4\mathrm{e}^{-\Omega_0/T}}{1+\mathrm{e}^{-\Omega_0/T}}-3\left[\frac{1+\left(\frac{S-1}{S}\right)^2\mathrm{e}^{-\Omega_0/T}}{1+\mathrm{e}^{-\Omega_0/T}}\right]^2\right\},$$

which are the desired susceptibilities incorporating the effects of finite population of the first excited levels.

The above results show that the corrections to the Ising limits $\chi_T=S^2/T$ and $\chi_{3T}=-S^4/3T^3$ are functionally exponential. This can be seen more explicitly as follows. Note first that $\beta\equiv\mathrm{e}^{-\Omega_0/T}$ is a small parameter in the considered approximation (for $\Omega_0\sim 15\mathrm{K}$ and $T\sim 5\mathrm{K}$, we have $\beta\sim 5\times 10^{-2}$). Then, introducing $f_k\equiv(1-1/S)^k$, the moments can be approximated binomially, $(1+x)^\alpha=1+\alpha x\cdots$, giving $\langle S_z^k\rangle=(1+\beta f_k)/(1+\beta)\simeq 1-\beta(1-f_k)$. To illustrate $1-f_2=(2S-1)/S^2$ gives explicitly

$$\chi_T=\frac{S^2}{T}\left[1-\left(\frac{2S-1}{S^2}\right)\mathrm{e}^{-\Omega_0/T}\right], \tag{A7}$$

and a result structurally similar for χ_{3T}. These exponential corrections are to be compared with the power-law corrections in the *classical* asymptotic results:[32]

$$\chi_T\simeq\frac{S^2}{T}\left(1-\frac{1}{\sigma}\right),\quad \chi_{3T}\simeq-\frac{S^4}{3T^3}\left(1-\frac{2}{\sigma}\right).$$

Thus, while in the classical case the corrections enter as inverse powers of $\sigma=DS^2/T$, for quantum spins they are exponential in D/T, leading to a much faster approach into the Ising regime as the temperature is lowered.

3. Dynamical nonlinear susceptibilities

Finally, we proceed to derive Eq. (12) for the frequency-dependent nonlinear susceptibility $\chi_3^{(\omega)}$ used in this work. The ordinary nonlinear susceptibility, denoted here $\chi_3^{(3\omega)}$, is defined in terms of the third harmonic of the response to an alternating field. For classical spins with uniaxial anisotropy a formula for $\chi_3^{(3\omega)}$ was derived[37] from a system of low-T balance equations[18] obtained from Brown's Fokker-Planck equation,[2] which reads

$$\chi_3^{(3\omega)}=-\frac{S^4}{3T^3}\left[\frac{b_\parallel^4}{1+3\mathrm{i}\omega\tau}-\frac{3\mathrm{i}\omega\tau(g_\parallel b_\parallel^4+g_\perp b_\parallel^2 b_\perp^2)}{2(1+\mathrm{i}\omega\tau)(1+3\mathrm{i}\omega\tau)}\right]. \tag{A8}$$

Here $b_\parallel=H_\parallel/H=\cos\psi$ and $b_\perp=H_\perp/H=\sin\psi$ are the direction cosines of the probing field, while $g_\parallel$ and $g_\perp$ are the expansion coefficients of the relaxation rate as given by Eq. (11), $\Gamma\simeq\Gamma_0\left[1+\frac{1}{2}(g_\parallel b_\parallel^2+g_\perp b_\perp^2)\xi^2\right]$, with $\Gamma_0=\Gamma|_{H=0}$ and $\xi=SH/T$ (these g's differ from those of Ref. 37 by a factor of 1/2). Accepting the validity of the balance equations for the number of spins pointing up or down, the derivation of Ref. 37 leading to Eq. (A8) is also valid for quantum spins (with uniaxial anisotropy).

An alternative nonlinear susceptibility,[10,11,14] the one we use in the main text, can be obtained from the first harmonic of the response in the presence of a weak static field H as $\chi(\omega,H)=\chi_1(\omega)+3\chi_3^{(\omega)}H^2+\cdots$ [cf. Eq. (1)]. Then, $\chi_3^{(\omega)}$ can be obtained from the first harmonic as

$$\partial_H^2\chi|_0 = 3!\chi_3^{(\omega)}. \tag{A9}$$

Experimentally, as discussed in Sec. II, one can measure χ for several H and get $\chi_3^{(\omega)}$ by polynomial fitting. Both $\chi_3^{(3\omega)}$ and $\chi_3^{(\omega)}$ coincide in the limit $\omega\to 0$ with the thermal equilibrium χ_{3T}. In addition, as we will see here, they have qualitatively similar dependences on the damping, ω, T, angle, etc. However, $\chi_3^{(\omega)}$ presents the experimental advantage of not requiring high-harmonic detection and processing.

To derive a formula for $\chi_3^{(\omega)}$ one can proceed as in Ref. 37 using a system of low-T balance equations. Here, however, we shall present a more direct derivation starting from the Debye form (2) for the first-harmonic response. Let us write this as $\chi(\omega,H)=\chi_S+\Delta\chi/1+i\omega\tau$, where $\Delta\chi=\chi_T-\chi_S$. This one-mode relaxation form is valid in weak enough fields,[45–47] just accounting for the H dependences of the χ's and τ. We can take advantage of this to get $\chi_3^{(\omega)}$ by simple differentiation $\chi_3^{(\omega)}=\partial_H^2\chi|_0/3!$. In addition, in the low-temperature regime we approximate the susceptibilities by their Ising limits (this is supported by the experiments of Sec. III). Consistently, the magnetization is given by $M_z/S=b_\parallel\tanh(\xi_\parallel)$, with $\xi_\parallel=b_\parallel\xi$. Then, we write the Debye law as

$$\chi(\omega,H)\simeq\frac{\Delta\chi}{1+i\omega\tau},\quad \Delta\chi\simeq\partial_H M_z. \tag{A10}$$

This low-T approximation entails to disregard $\chi_S\ll\chi_T-\chi_S$ and $\partial_H^2\chi_S\ll\chi_{3T}$,[32] and corresponds to the two-state approximation in the balance equation approach.[37]

Based on the above considerations we simply write

$$\chi=(\partial_H M_z)D,\quad D=\frac{\Gamma}{\Gamma+i\omega}, \tag{A11}$$

and proceed to differentiate to get $\chi_3^{(\omega)}=\partial_H^2\chi|_0/3!$, using eventually $\Gamma=\Gamma_0(1+Q\xi^2/2)$. To work out the second derivative we use the "binomial" formula $(fg)''=f''g+2f'g'+fg''$, which results in

$$\partial_H^2\chi=(\partial_H^3 M_z)D+2\partial_H^2 M_z\partial_H D+\partial_H M_z\partial_H^2 D. \tag{A12}$$

Now, using the evenness of the rate on H, we have $\partial_H\Gamma|_0=0$, which has two important consequences

$$\partial_H D|_0=0,\quad \partial_H^2 D|_0=\left.\frac{i\omega\partial_H^2\Gamma}{(\Gamma+i\omega)^2}\right|_0.$$

Then, from $\Gamma=\Gamma_0(1+Q\xi^2/2)$ and $\partial_H=(S/T)\partial_\xi$, along with $\partial_H M_z|_0=\chi_T$ and $\partial_H^3 M_z|_0=3!\chi_{3T}$, we finally obtain

$$\chi_3=\frac{\chi_{3T}}{1+i\omega\tau}+\frac{\chi_T S^2}{T^2}\frac{i\omega\tau Q}{6(1+i\omega\tau)(1+i\omega\tau)}, \tag{A13}$$

where now $\tau=1/\Gamma_0$ is the zero-field relaxation time.

To compare with Eq. (A8) for $\chi_3^{(3\omega)}$, we recall that $M_z/S=b_\parallel\tanh(\xi_\parallel)$ and use the expansion $\tanh\xi\simeq\xi-\frac{1}{3}\xi^3$, whence $\partial_H M_z=(S^2/T)(b_\parallel^2-b_\parallel^4\xi^2)$ and $\partial_H^3 M_z|_0=6(-S^4 b_\parallel^4/3T^3)$. Then, introducing the explicit expression for $Q=g_\parallel b_\parallel^2+g_\perp b_\perp^2$, we arrive at [cf. Eq. (12)]

$$\chi_3^{(\omega)}=-\frac{S^4}{3T^3}\left[\frac{b_\parallel^4}{1+i\omega\tau}-\frac{i\omega\tau(g_\parallel b_\parallel^4+g_\perp b_\parallel^2 b_\perp^2)}{2(1+i\omega\tau)(1+i\omega\tau)}\right]. \tag{A14}$$

This result is generic and valid for classical and quantum spins, inasmuch as the starting Debye χ provides an adequate description. In general, $g_\parallel$ and $g_\perp$ will not be given by the classical result (13), but they incorporate quantum contributions to the relaxation rate.

The expression derived for $\chi_3^{(\omega)}$ shows a close structural analogy with that for the third-harmonic nonlinear susceptibility [cf. Eq. (A14) with Eq. (A8)]. Indeed, we have kept the factor $(1+i\omega\tau)^2$ without squaring in Eq. (A14) to enhance the analogy; replacing $\omega\tau\to 3\omega\tau$, both quantities exhibit almost the same frequency dependence. Comparison of Eq. (A14) with Eq. (A8) also reveals similar dependences on T, $g_\parallel$, and $g_\perp$, as well as on the angle ψ. This supports our repeated claim about the analogous qualitative dependences of $\chi_3^{(3\omega)}$ and $\chi_3^{(\omega)}$ and, in turn, our choice of the first harmonic response on the basis of its experimental convenience.

We conclude this appendix finding extrema and zeros of $\chi_3(\omega)$. This will help to exploit having an analytical expression for the nonlinear susceptibility when analyzing experiments. First we normalize Eq. (A14) by the equilibrium value $\tilde{\chi}_3=\chi_3^{(\omega)}/\chi_{3T}$:

$$\tilde{\chi}_3=\frac{1}{1+ix}-\frac{\bar{Q}}{2}\frac{ix}{(1+ix)^2},\quad x=\omega\tau, \tag{A15}$$

where $\bar{Q}=Q/b_\parallel^2=g_\parallel+g_\perp(b_\perp/b_\parallel)^2$. Multiplying now by the conjugate denominators we readily separate the real and imaginary parts

$$\tilde{\chi}_3'=\frac{1}{1+x^2}-\frac{\bar{Q}x^2}{(1+x^2)^2},\quad -\tilde{\chi}_3''=\frac{x}{1+x^2}+\frac{\bar{Q}}{2}\frac{x(1-x^2)}{(1+x^2)^2}.$$

Let us first compute where the imaginary part crosses the $\omega\tau$ axis (see Fig. 6, bottom panel). To find this requires to solve $x(1+x^2)+(\bar{Q}/2)x(1-x^2)=0$. Apart from $x=0$, one finds the following zero:

$$x_z^2=\frac{\bar{Q}+2}{\bar{Q}-2}\quad\overset{|\bar{Q}|\gg 1}{\rightsquigarrow}\quad x_z\simeq 1+\frac{2}{\bar{Q}}. \tag{A16}$$

To get the large-$\bar{Q}$ approximation we have used the binomial formula $(1+x)^\alpha=1+\alpha x\cdots$ twice (to work the denominator and then to take the square root). Well, note that for $|\bar{Q}|<2$ one has $x_z^2<0$ and hence the imaginary part does not cross the x axis. However, when one *finds* the crossing, the following criterion holds: if $x_z>1$, then $\bar{Q}>0$, whereas for $x_z<1$, one has $\bar{Q}<0$. Thus, inspection of the crossing of the $\omega\tau$ axis (below or above $\omega\tau=1$) could provide information on the classical or quantum character of the spin-reversal dynamics.

Let us now find the extrema x_m of the real part $\tilde{\chi}_3'$. Writing $\tilde{\chi}_3'=[1+(1-\bar{Q})x^2]/(1+x^2)^2$ one sees that $d\tilde{\chi}_3'/dx=0$ implies $-(1+\bar{Q})+(1-\bar{Q})x_m^2=0$, whence

$$x_{\mathrm{m}}^2 = \frac{\bar{Q}+1}{\bar{Q}-1} \quad \overset{|\bar{Q}|\gg 1}{\rightsquigarrow} \quad x_{\mathrm{m}} \simeq 1 + \frac{1}{\bar{Q}}. \tag{A17}$$

There is a maximum, or minimum, when $|\bar{Q}|>1$: in such a case, $x_{\mathrm{m}}>1$ entails $\bar{Q}>0$, whereas $x_{\mathrm{m}}<1$ yields $\bar{Q}<0$. We conclude giving the value of $\tilde{\chi}_3'$ at its extremum:

$$\tilde{\chi}_3'(x_{\mathrm{m}}) = -\frac{(\bar{Q}-1)^2}{4\bar{Q}} \quad \overset{|\bar{Q}|\gg 1}{\rightsquigarrow} \quad \tilde{\chi}_3'(x_{\mathrm{m}}) \simeq -\frac{\bar{Q}}{4}, \tag{A18}$$

which is the result used in Sec. IV to get $g_{\parallel}$ from the maximum of $\tilde{\chi}_3'$ at $\psi=0$ (then $\bar{Q}=g_{\parallel}$). Note finally that the signs of the $\tilde{\chi}_3'$ peak and of $\bar{Q}$ are *always* opposite, which can help ascertaining the quantum contribution to the nonlinear dynamics.

[1] Q. A. Pankhurst and R. J. Pollard, J. Phys.: Condens. Matter **5**, 8487 (1993).

[2] W. F. Brown, Jr., Phys. Rev. **130**, 1677 (1963).

[3] These are described by the stochastic Landau-Lifshitz equation or its Fokker-Planck counterpart for the probability distribution of spin orientations (Ref. 2).

[4] F. Hartmann-Boutron, P. Politi, and J. Villain, Int. J. Mod. Phys. B **10**, 2577 (1996).

[5] W. H. Zurek, Phys. Today **44**(10), 36 (1991).

[6] A. J. Leggett, J. Phys.: Condens. Matter **14**, R415 (2002).

[7] U. Weiss, *Quantum Dissipative Systems* (World Scientific, Singapore, 1993).

[8] S. J. Blundell and F. L. Pratt, J. Phys.: Condens. Matter **16**, R771 (2004).

[9] N. Hegman, L. F. Kiss, and T. Kemény, J. Phys.: Condens. Matter **6**, L427 (1994).

[10] P. Schiffer, A. P. Ramirez, D. A. Huse, P. L. Gammel, U. Yaron, D. J. Bishop, and A. J. Valentino, Phys. Rev. Lett. **74**, 2379 (1995).

[11] W. Wu, D. Bitko, T. F. Rosenbaum, and G. Aeppli, Phys. Rev. Lett. **71**, 1919 (1993).

[12] R. Harris, M. Plischke, and M. J. Zuckermann, Phys. Rev. Lett. **31**, 160 (1973).

[13] T. Bitoh, K. Ohba, M. Takamatsu, T. Shirane, and S. Chikazawa, J. Phys. Soc. Jpn. **62**, 2583 (1993).

[14] T. Jonsson, P. Svedlindh, and M. F. Hansen, Phys. Rev. Lett. **81**, 3976 (1998).

[15] P. Jönsson, T. Jonsson, J. L. García-Palacios, and P. Svedlindh, J. Magn. Magn. Mater. **222**, 219 (2000).

[16] J. L. García-Palacios, P. Jönsson, and P. Svedlindh, Phys. Rev. B **61**, 6726 (2000).

[17] J. L. García-Palacios and P. Svedlindh, Phys. Rev. Lett. **85**, 3724 (2000).

[18] D. A. Garanin, E. C. Kennedy, D. S. F. Crothers, and W. T. Coffey, Phys. Rev. E **60**, 6499 (1999).

[19] F. Luis, V. González, A. Millán, and J. L. García-Palacios, Phys. Rev. Lett. **92**, 107201 (2004).

[20] See, for instance, H. Mamiya, I. Nakatani, and T. Furubayashi, Phys. Rev. Lett. **88**, 067202 (2002), and references therein.

[21] J. R. Friedman, M. P. Sarachik, J. Tejada, and R. Ziolo, Phys. Rev. Lett. **76**, 3830 (1996).

[22] J. M. Hernández, X. X. Zhang, F. Luis, J. Bartolomé, J. Tejada, and R. Ziolo, Europhys. Lett. **35**, 301 (1996).

[23] L. Thomas, F. Lionti, R. Ballou, D. Gatteschi, R. Sessoli, and B. Barbara, Nature (London) **383**, 145 (1996).

[24] D. A. Garanin and E. M. Chudnovsky, Phys. Rev. B **56**, 11 102 (1997).

[25] F. Luis, J. Bartolomé, and J. F. Fernández, Phys. Rev. B **57**, 505 (1998).

[26] A. Würger, J. Phys.: Condens. Matter **10**, 10075 (1998).

[27] T. Lis, Acta Crystallogr., Sect. B: Struct. Crystallogr. Cryst. Chem. **36**, 2042 (1980).

[28] The large constant χ' at high ω does not reveal a large χ_S, but it corresponds to the χ_T of a minority fraction of clusters with different magnetic parameters (lower D) due to thermodynamic defects. For a discussion on the nature of these defects see, for instance, Z. Sun, D. Ruiz, N. R. Dilley, M. Soler, J. Ribas, K. Folting, B. Maple, G. Christou, and D. N. Hendrickson, Chem. Commun. (Cambridge) **19**, 1973 (1999).

[29] P. E. Jönsson and J. L. García-Palacios, Phys. Rev. B **64**, 174416 (2001).

[30] R. L. Carlin, *Magnetochemistry* (Springer, Berlin, 1986).

[31] A.-L. Barra, D. Gatteschi, and R. Sessoli, Phys. Rev. B **56**, 8192 (1997).

[32] J. L. García-Palacios, Adv. Chem. Phys. **112**, 1 (2000).

[33] For random axes the decrease of $\chi_T/\chi_{\mathrm{iso}}$ by the small factor $S^2/S(S+1)\simeq 0.91$ is probably compensated by interaction effects.

[34] D. Ruiz-Molina, M. Más-Torrent, J. Gómez, A. Balana, N. Domingo, J. Tejada, M. T. Martínez, C. Rovira, and J. Veciana, Adv. Mater. (Weinheim, Ger.) **15**, 42 (2003); A. Cornia, R. Sessoli, L. Sorace, D. Gatteschi, A. L. Barra, and C. Daiguebonne, Angew. Chem., Int. Ed. **42**, 1645 (2003); M. Cavallini, F. Biscarini, J. Gómez, D. Ruiz-Molina, and J. Veciana, Nano Lett. **11**, 1527 (2003).

[35] M. Clemente-León, E. Coronado, A. Forment-Aliaga, P. Amorós, J. Ramírez-Castellanos, and J. M. González-Calbet, J. Mater. Chem. **13**, 3089 (2003).

[36] For the classical calculations, we use the simplest uniaxial anisotropy $\mathcal{H}=-DS_z^2$ but with a barrier $U=70$ K, equal to that provided by Hamiltonian (7).

[37] J. L. García-Palacios and D. A. Garanin, Phys. Rev. B **70**, 064415 (2004).

[38] P. E. Jönsson and J. L. García-Palacios, Europhys. Lett. **55**, 418 (2001).

[39] The relaxation rate Γ should be invariant upon field inversion, leading to the absence of odd powers in the field expansion (11); the invariance of Γ upon field reflection through the barrier plane yields the vanishing of a mixed term $\propto\xi_{\parallel}\xi_{\perp}$ for uniaxial spins.

[40] J. R. Friedman, M. P. Sarachik, and R. Ziolo, Phys. Rev. B **58**, R14729 (1998).

[41] I. Tupitsyn and B. Barbara, in *Magnetism: Molecules to Materials*, edited by J. S. Miller and M. Drillon (Wiley-VCH, Weinheim, 2002), Vol. III, pp. 109–168.

[42] F. Luis, F. Mettes, and L. J. de Jongh, in *Magnetism: Molecules to Materials*, edited by J. S. Miller and M. Drillon (Wiley-VCH, Weinheim, 2002), Vol. III, pp. 169–210.

[43] J. F. Fernández, F. Luis, and J. Bartolomé, J. Appl. Phys. **83**, 6940 (1998).

[44] Dipole-dipole interactions between molecular spins could in principle contribute to decoherence. Experimental evidence, however, shows that the broadening of the Mn_{12} excited levels is predominantly homogeneous [see Ref. 40, and W. Wernsdorfer, R. Sessoli, and D. Gatteschi, Europhys. Lett. **47**, 254 (1999)]. Therefore, the decoherence mechanism considered here is probably giving the dominant contribution.

[45] J. F. Fernández, F. Luis, and J. Bartolomé, Phys. Rev. Lett. **80**, 5659 (1998).

[46] T. Pohjola and H. Schoeller, Phys. Rev. B **62**, 15026 (2000).

[47] D. Zueco and J. L. García-Palacios, cond-mat/0509627 (unpublished).